


EXPRESS LETTER

Open Access



Tomographic image of crust and upper mantle off the Boso Peninsula using data from an ocean-bottom seismograph array

Aki Ito^{1*} , Yojiro Yamamoto², Ryota Hino³, Daisuke Suetsugu¹, Hiroko Sugioka⁴, Masaru Nakano², Koichiro Obana², Kazuo Nakahigashi⁵ and Masanao Shinohara⁶

Abstract

We determined the three-dimensional structure of the crust and upper mantle off the Boso Peninsula, Japan, by analyzing seismograms recorded by ocean-bottom seismometers and land stations between 2011 and 2013. We employed seismic tomography to determine the P- and S-wave velocity structures and earthquake locations simultaneously. The tomographic image shows that the mantle parts of the Pacific and the Philippine Sea plates have high-velocity anomalies. The upper boundary of the Philippine Sea plate is delineated as approximately 2–6 km shallower than that previously estimated from land-based data for the area 140.5°E–141.5°E and 35°N–35.5°N. A pronounced low-velocity anomaly in P- and S-waves with low- V_p/V_s ratio (1.5–1.6) was observed at depths shallower than 20 km in the overriding North American plate. This anomaly may be caused by the presence of rocks with a low- V_p/V_s ratio, such as quartzite, and the water expelled from the subducted Pacific and Philippine Sea plates.

Keywords: Boso Peninsula, Philippine Sea plate, North American plate, Three-dimensional velocity structure, Ocean-bottom observation

Background

The region off the Boso Peninsula, Japan, is an oceanic area with a trench–trench–trench triple junction (Fig. 1a), where the Pacific plate (PAC) is subducted westward from the Japan Trench beneath the North American plate (NA) and the Philippine Sea plate (PHS) is subducted northwestward beneath the NA from the Sagami trough (DeMets et al. 2010). The PHS contacts and overrides the PAC beneath this region (Ishida 1992), and its northeastern limit is determined based on the slip directions of interplate earthquakes (Uchida et al. 2009). The upper boundary of the PHS is located at depths of 10–30 km beneath the Boso Peninsula (Uchida et al. 2010). The upper boundary of the subducted PAC has been determined based on relocated hypocenter

distributions (Nakajima et al. 2009). Because these plate boundaries mainly used data from land-based stations, the plate geometries beneath the offshore area have not been reliably defined.

The region off the Boso Peninsula is characterized by various seismic and geodetic activities associated with the PHS, including the 1703 Genroku-Kanto earthquake (M 7.9–8.2) and the 1923 Kanto earthquake (M_w 7.9) (Matsu'ura et al. 2007; Sato et al. 2016), and slow slip events (Hirose et al. 2014). Further, this region is extremely important with respect to the risk assessment of earthquakes and tsunamis, as it is located less than 100 km away from the Tokyo metropolitan area.

Despite the importance of these data from scientific and disaster prevention viewpoints, the three-dimensional structure of the crust and upper mantle beneath the region off the Boso Peninsula remains poorly understood. Extensive tomographic studies have been performed on the region beneath central Japan, including the Boso Peninsula (Kamiya and Kobayashi 2000; Matsumura et al. 2005; Nakajima et al. 2009). The subducting

*Correspondence: iaki@jamstec.go.jp

¹ Department of Deep Earth Structure and Dynamics Research, Japan Agency of Marine-Earth Science and Technology, 2-15 Natsushima-cho, Yokosuka, Kanagawa 237-0061, Japan

Full list of author information is available at the end of the article

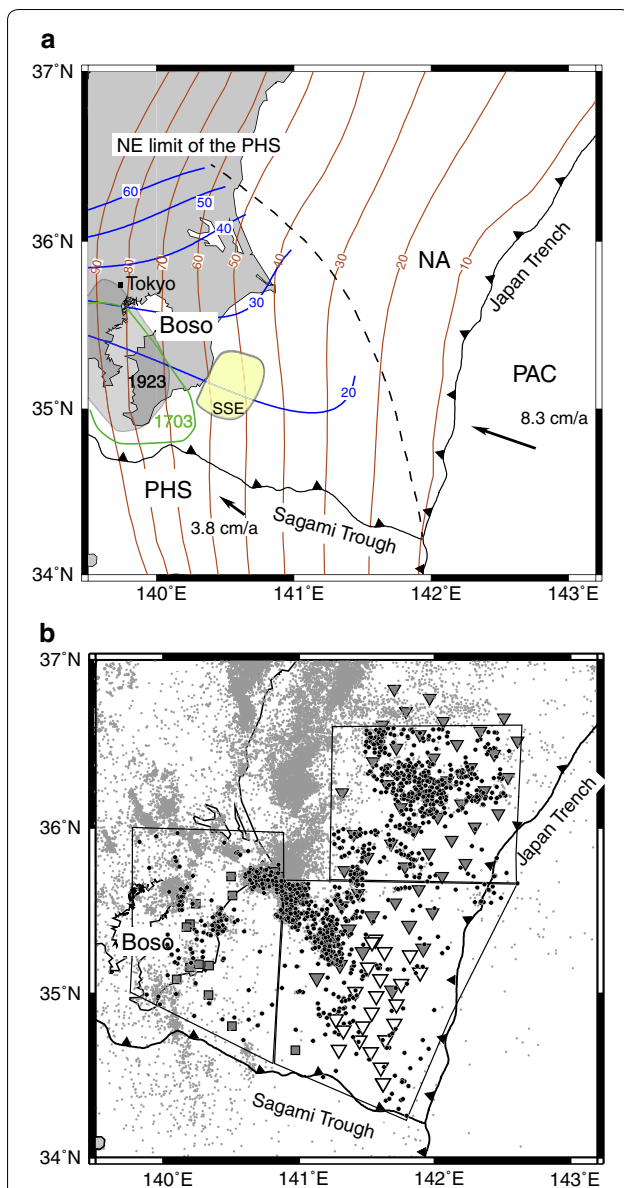


Fig. 1 Tectonic setting of the study area and locations of seismic stations. **a** Blue and brown contours show the depths of upper boundaries of the PHS (Uchida et al. 2010) and the PAC (Nakajima et al. 2009), respectively. The black dashed line denotes the northeastern limit of the PHS (Uchida et al. 2009). Source areas of the 1703 Genroku Kanto and 1923 Kanto earthquakes are indicated by gray and green lines, respectively (Matsu'ura et al. 2007; Sato et al. 2016). The area of slow slip events is shown in yellow (Hirose et al. 2014). Black lines with triangles represent trench axes. Black arrows indicate the motion of PAC and PHS with respect to the NA (DeMets et al. 2010). **b** Locations of seismic stations. White and gray triangles indicate OBSs of JAMSTEC and ERI, respectively, while gray squares indicate stations operated by NIED. Small gray dots are earthquake epicenters determined by JMA between October 2011 and March 2013. Earthquake selection areas are delineated by black lines while black dots are epicenters determined by JMA and analyzed in this study

PHS and PAC have been imaged with high velocity, and the existence of the low velocities region with high Poisson's ratio has been suggested in the mantle of the NA, which are associated with the serpentinized periodite. However, these studies did not cover the region off the Boso Peninsula, primarily because of a lack of data in the oceanic area.

Several offshore refraction studies have been performed to determine the crustal structure (Nakahigashi et al. 2012; Kono et al. 2017); however, these studies have allowed only two-dimensional model along the survey lines to be constructed.

To determine the three-dimensional structure beneath the region, seismic observations using ocean-bottom seismometers (OBS) are necessary. Although several seismic observations have been conducted beneath a region off Miyagi (Yamamoto et al. 2014), few seismic observations have been conducted with OBS off the Boso Peninsula before 2011 and consequently no three-dimensional structures have been revealed, particularly south of 35.5°N.

Several OBS studies were performed in the aftershock area of the 2011 Tohoku-oki earthquake (Shinohara et al. 2012; Ito et al. 2017). Ito et al. (2017) analyzed the location and focal mechanism of the earthquakes in the region, in order to determine the boundaries of the PHS and the NA. They found that the depth of the plate upper boundary of the PHS off the Boso Peninsula is approximately 6 km shallower than that previously estimated by Uchida et al. (2010) at approximately 141.0°E.

In the present study, we determined the three-dimensional P- and S-velocity structures of the crust and upper mantle beneath the region off the Boso Peninsula using seismic tomography, in order to elucidate the spatial geometries of the three plates and the velocity anomalies.

Data and methods

Data

We used data from temporary seismic observations performed using OBSs by the Japan Agency of Marine-Earth Science and Technology (JAMSTEC) and the Earthquake Research Institute (ERI) of the University of Tokyo. Observations using a total of 23 OBSs were performed by JAMSTEC for a year starting in March 2012 (Ito et al. 2017). The ERI also conducted seismic observations from October 2011 to November 2012 across a broad area of the Japan Trench forearc region (Shinohara et al. 2012). We used seismic data from 50 of ERI OBSs to cover the northern part of the Boso offshore area. In addition to the data from these OBS stations, we also used seismic data from 12 land seismic stations and 3 seismic stations on the offshore area operated by the National Research

Institute for Earth Science and Disaster Prevention (NIED) (Okada et al. 2004). The observation period, the number of stations, and their locations are given in Additional file 1: Table A1 and Fig. 1b.

We selected approximately 1400 earthquakes that occurred between October 2011 and March 2013 from the Japan Meteorological Agency (JMA) catalog; the magnitudes of these earthquakes ranged from 1.1 to 6.3. To select the earthquakes, we delineated three regions where we expected the velocity structure to be well constrained by our dataset (Fig. 1b). Of the earthquakes located within these three regions, we selected those for which at least ten arrival data could be identified in the record.

We picked the onset times for the arrival of the P- and S-waves manually from the vertical and horizontal components of the OBS data. For the seismic stations by NIED, we collected the arrival data of the P- and S-waves from the catalog by NIED.

Hypocenter location

We used the JMA2001 velocity model, which is a standard velocity model for the Japanese Islands (Ueno et al. 2002) (Fig. 2a), to relocate the initial hypocenters for use in a tomographic inversion. Because the focal depths determined by JMA are generally deeper than the hypocenters relocated with OBS data (Ito et al. 2017), we conducted relocation to obtain more appropriate initial hypocenters for tomography. When we investigate seismic structure by using OBS data, it is necessary to take effect of slow sedimentary layers in an oceanic area into account. We introduced station correction terms based on PS converted phases following the methods of previous OBS studies (Hino et al. 2000). The calculation of station corrections is detailed in Additional file 1: Additional note 1.

We used NonLinLoc software (Lomax et al. 2000), which is based on a grid-search algorithm, to determine locations and origin times of the earthquakes using the arrival data of the P- and S- waves. The spacing of the grid nodes in the velocity model was assumed to be 1 km. Figure 2b shows the 1288 earthquakes relocated with an error of less than 2 km in the horizontal direction and less than 3 km along the depth direction. The RMS values of the travel time residuals for the P-wave and S-wave arrival times are 0.43 and 0.90 s, respectively.

Seismic tomography

We used the program tomoDD (Zhang and Thurber 2003) to determine the three-dimensional P- and S-wave velocity structures and the locations and origin times of the hypocenters simultaneously using the

double-difference tomography method. We introduced the same station correction terms as the initial hypocenters location.

We estimated the V_p/V_s ratios from the P- and S-velocities. The initial velocity model was the one used to determine the initial hypocenter locations (Fig. 2a). The horizontal locations in the model space were expressed using the orthogonal coordinates X and Y in the Japan Trench-normal and Trench-parallel directions, respectively (Fig. 2c). We set a grid with nodes spaced at intervals of 20 km along the X and Y coordinates, which were chosen by an average spacing of OBS stations. In the vertical direction, intervals of 5 km were used for all depths.

The input data were the absolute arrival and differential travel times. We used 31,740 and 16,729 data for the absolute arrival times of the P- and S-waves, respectively, and 68,934 and 31,638 data for the differential times calculated by manually picking data for the P- and S-waves for event pairs within 10 km, respectively (Waldhauser and Ellsworth 2000).

Several parameters have to be chosen when performing tomography. These include the weight of the differential travel time data with respect to the absolute arrival time data; the relative weights of the P- and S-wave data; and the damping and smoothing parameters. We described the ways to select those parameters in Additional note 2. After 18 iterations of the tomographic inversion, the RMS of the total travel time residuals was reduced from 0.50 to 0.25 s. The decrease in the travel time residuals for each data type is shown in Additional file 1: Table A2.

We performed a checkerboard resolution test (CRT) (Spakman and Nolet 1988), to evaluate the spatial resolution of the velocity model. Almost the entire region off the Boso Peninsula is resolved at depths shallower than 30 km for the P- and S-waves. The spatial patterns for wavelengths greater than 40 km in the horizontal and 10 km in the vertical directions were robust (see Additional file 1: additional note 3).

Results

Pacific plate

Figures 3, 4, and 5a show the results of the tomographic inversion in the horizontal and vertical sections. The velocity models are shown by the absolute velocities. Unresolved areas, which were determined by the derivative weight sum values (DWS) (Thurber and Eberhart-Phillips 1999), are masked (see Additional file 1: Additional note 3). For the V_p/V_s ratios, the resolved areas are assumed to be same as those for the S-wave, since the resolved area for V_p includes that for V_s .

The tomographic image shows the mantle part of the PAC plate. It is imaged at depths of 20–30 km in

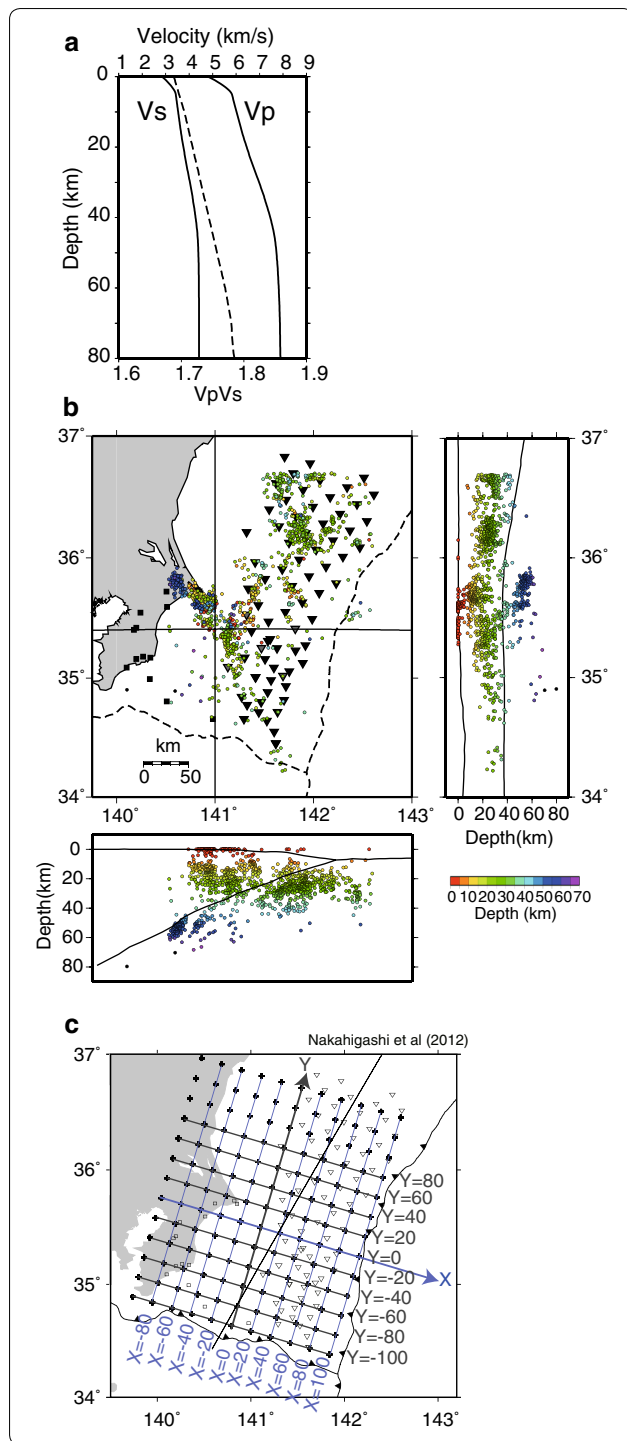


Fig. 2 Initial velocity model and hypocenter distribution and grid configuration during tomographic inversions. **a** One-dimensional JMA2001 velocity model (Ueno et al. 2002) used for initial hypocenter determination and initial model for tomographic inversion. *Bold* and *dashed lines* show the velocities and V_p/V_s ratio of the model. **b** Relocated hypocenters based on the one-dimensional model shown in (a). *Colored dots* represent hypocenters. *Colors* indicate hypocenter depth. *Black triangles* and *squares* indicate station locations. *Lower* and *right-hand panels* show E–W and N–S vertical sections, respectively. PAC upper boundaries (Nakajima et al. 2009) are shown along the latitude of 35.4°N and longitude of 141°E, on the E–W and N–S vertical sections, respectively. **c** Configuration of grid nodes during tomographic inversions. *Crosses* represent locations of velocity nodes in horizontal section. *Triangles* and *squares* indicate the locations of stations. *Black bold line* shows the locations of refraction survey (Nakahigashi et al. 2012)

estimated V_p and V_s values are 7.5–8.3 and 4.3–4.8 km/s, respectively. The velocities of the mantle part of the PAC are consistent with those obtained by Nakajima et al. (2009), who estimated the V_p and V_s values of the mantle part of the PAC to be 7.5–8.3 and 4.5–4.7 km/s, respectively, at depths greater than 50 km beneath the Boso Peninsula, using land-based data.

Philippine Sea plate

The mantle part of the PHS was also imaged in terms of the high-velocity anomalies in the P wave at depths of 25–30 km in the horizontal sections (Fig. 3). It is evident from the vertical profiles that the mantle part of the PHS is subducted northward at -40 to -20 in the X axis in the N–S cross-sections (Fig. 5a). The high-velocity anomalies associated with the PHS are located at depths of approximately 25–40 km, roughly along the upper boundary of the PHS after Uchida et al. (2010). The V_p values of the mantle part of the PHS were estimated to be 7.5–8.0 km/s, which is consistent with those estimated by the previous tomographic studies using land-based data ($V_p = 7.5$ –8.2 km/s) at depths of >30 km (Matsubara et al. 2005; Nakajima et al. 2009). The high-velocity anomalies are outside the resolved area in the S-velocity model, probably because of the relative paucity of S-wave data.

There is a region of $V_p = 6.5$ –7.5 km/s (labeled “A” in Figs. 4, 5a) atop the mantle part of the PHS in the vertical section. The V_p values of region A are faster than those of the lower crust of the NA ($V_p = 6.3$ –6.5 km/s), as determined from a refraction study along the survey line shown in Fig. 2c (Nakahigashi et al. 2012). Region A has a thickness of 10–12 km (between iso-velocity contours of 6.5 and 7.5 km/s). We consider region A to be the crustal part of the PHS, which will be discussed later.

the horizontal sections in terms of the high-velocity anomalies in the P- and S-waves that are shifted westward with depth (Fig. 3). In the E–W vertical profiles (Fig. 4), the high-velocity anomalies associated with the PAC are located at depths of 20–40 km just below the upper boundary of the PAC (Nakajima et al. 2009). The

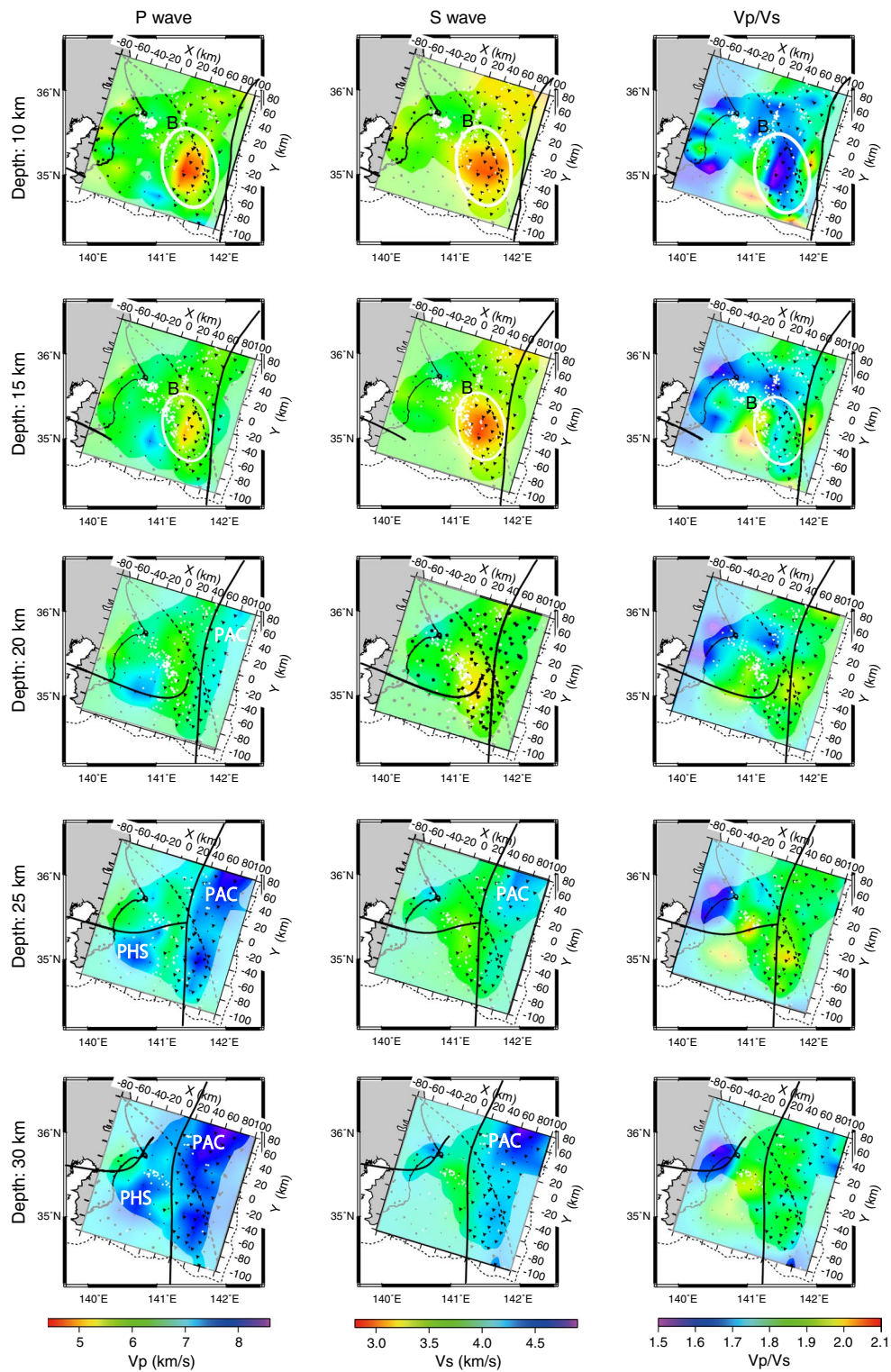


Fig. 3 Results of the tomographic inversion in horizontal section. Velocity structures for P-wave (left), S-wave (middle), and V_p/V_s (right) are shown. Black triangles and squares indicate stations. White circles indicate earthquakes within 10 km from each section. Black crosses represent the locations of velocity nodes. Black bold lines indicate the location of the upper boundaries of the PAC (Nakajima et al. 2009) and PHS (Uchida et al. 2010) at each depth. The black dashed line denotes the northeastern limit of the PHS (Uchida et al. 2009). High-velocity anomalies associated with the mantle part of the PAC and PHS are indicated by "PAC" and "PHS," respectively. The low-velocity anomaly in the NA plate is indicated by the white circle labeled "B."

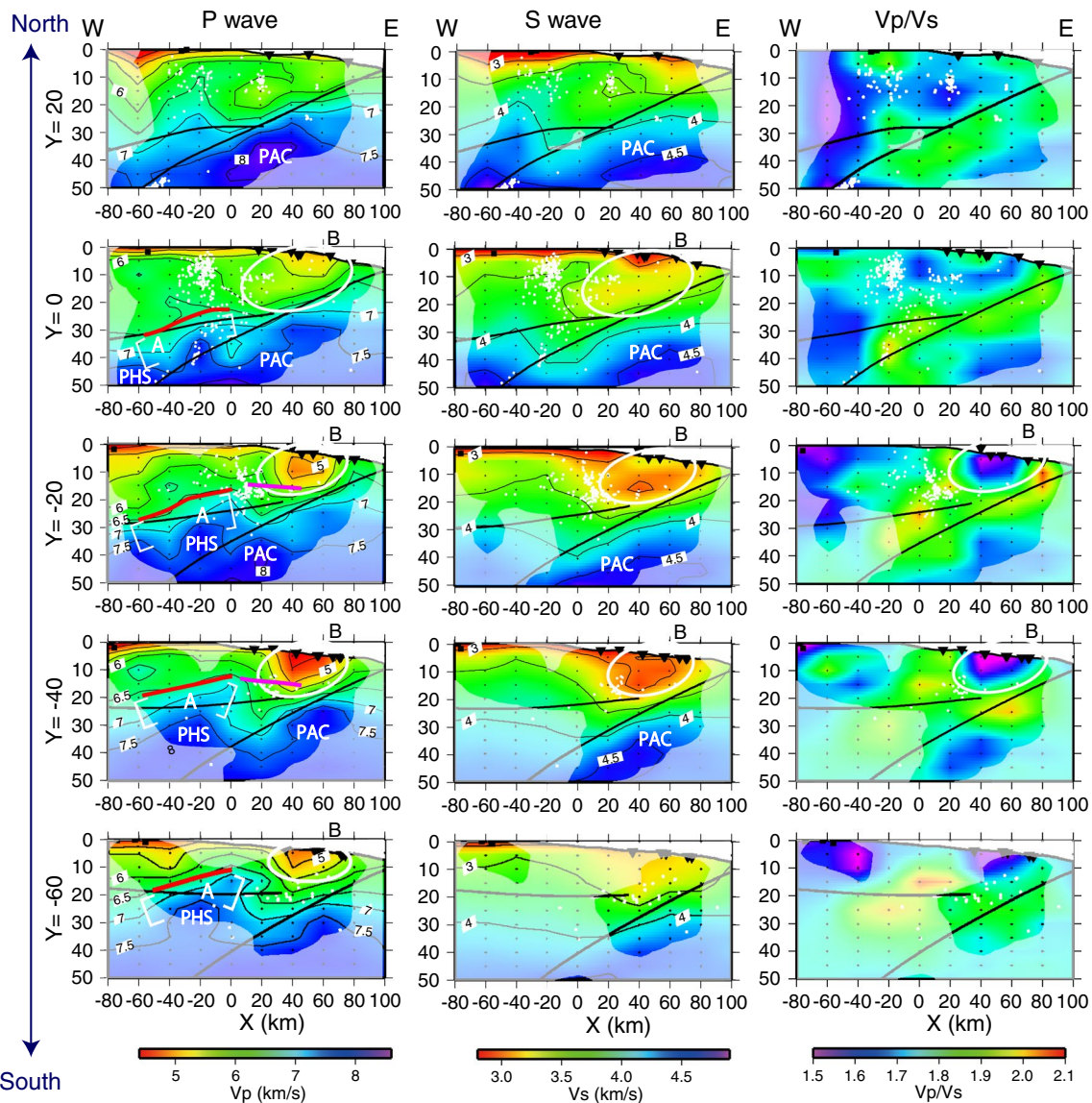


Fig. 4 Vertical profiles of velocity structure along the X axis shown in Fig. 2c. The contour interval of the velocity is 0.5 km/s. Black triangles and squares, and white circles indicate the locations of stations and earthquakes within 10 km from each section, respectively. Black bold lines indicate the location of the upper boundaries of the PAC (Nakajima et al. 2009) and PHS (Uchida et al. 2010). Red and magenta lines show the upper boundary of the PHS based on the present tomographic image and result of Ito et al. (2017), respectively. The crustal part of the PHS is indicated by areas labeled A. The other symbols are same as those defined in Fig. 3

Low-velocity zone in the NA

A pronounced low-velocity anomaly in the P- and S-waves was observed at depths ≤ 20 km near the Japan Trench (indicated by a white circle labeled “B” in Figs. 3, 4, 5a). The northern edge of the region almost coincides with the northeastern limit of the PHS (Uchida et al. 2009) at 20–80 km in the X axis in the horizontal sections (Fig. 3). In the E–W profiles (Fig. 4), region B is located above the upper boundary of the PHS at –60 to 0 km in the Y axis. Region B has V_p and V_s values of 4.4–5.5 km/s

and 2.8–3.5 km/s, respectively. The V_p/V_s ratio is estimated to be 1.5–1.6 at depths shallower than 15 km, where both V_p and V_s are well resolved.

Discussion

Upper boundary of the PHS

We ascribed region A, immediately above the mantle part of the PHS, to the crustal part of the PHS. Although the crustal part is difficult to discuss in detail because of the spatial resolution of the vertical

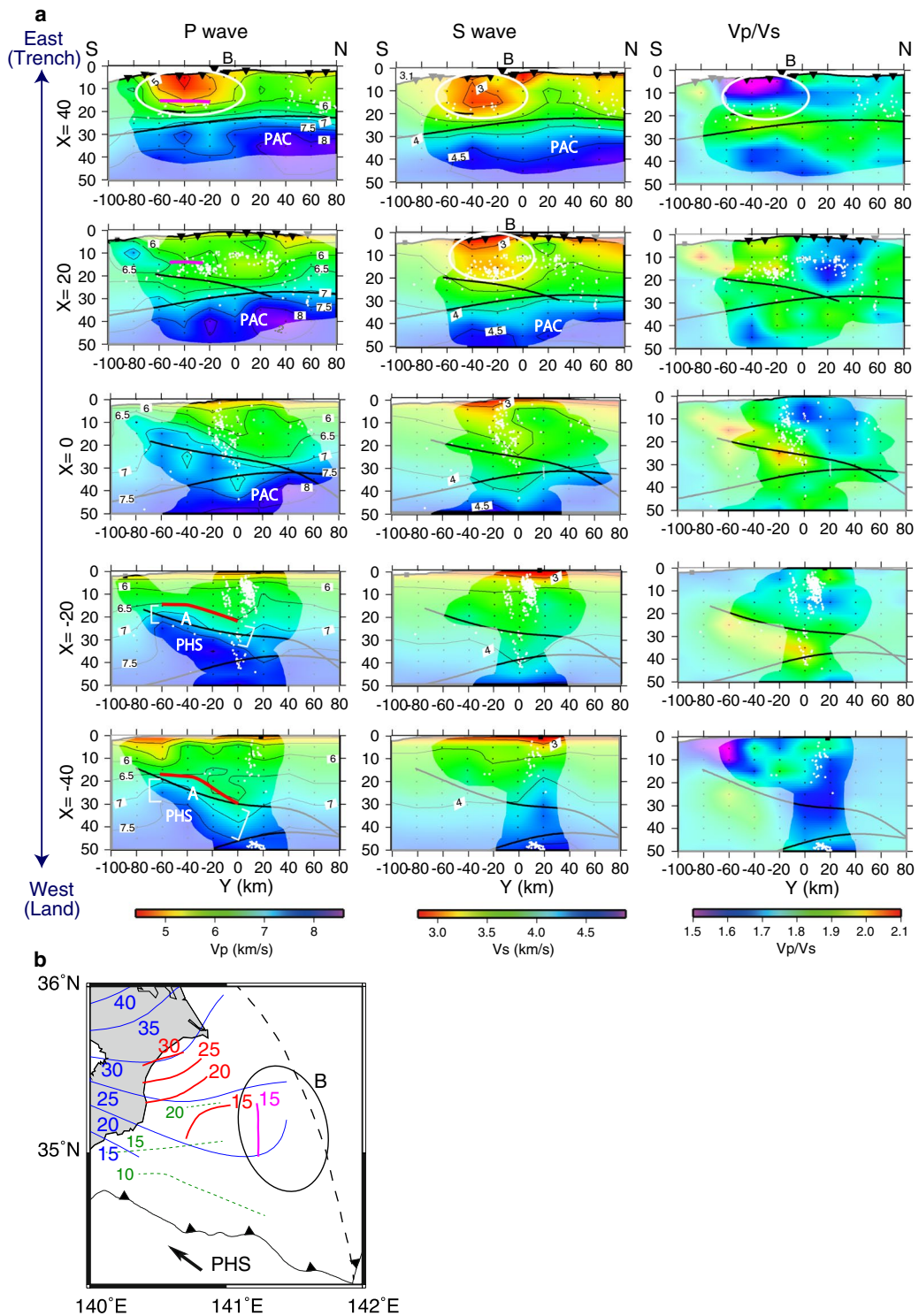


Fig. 5 Vertical profiles of velocity structure and geometries of the upper boundary of the PHS. **a** Vertical profiles of velocity structure along the Y axis shown in Fig. 2c. **b** Geometries of the upper boundary of the PHS. Red and magenta lines show the depths of the upper boundary of the PHS based on the tomographic image and results by Ito et al. (2017), respectively. Blue and green dotted contours show depths of the upper boundaries of the PHS estimated by Uchida et al. (2010) and compiled by Kono et al. (2017). The location of the low-velocity anomaly in the NA plate is indicated by the black circle labeled “B.”

direction, the thickness (10–12 km) and the V_p values (6.5–7.5 km/s) are almost consistent with those estimated by Matsubara et al. (2005), who estimated a thickness and V_p of the subducted PHS crust to be 10–12 and 6.4–7.5 km/s, respectively, at depths of 30–70 km beneath the Kanto region. The top of region A, which is represented by smoothed iso-velocity contour of 6.5 km/s, is shown on the vertical sections (Figs. 4, 5a) and on the horizontal section (Fig. 5b). Assuming the top of the PHS crust corresponds to the upper boundary of the PHS, the upper boundary is dipping toward the northwest, which is nearly parallel to the convergent direction of the PHS. We also draw the upper boundary of the PHS east of region A as determined from hypocenter distributions and focal mechanisms (Ito et al. 2017). The upper boundaries of the PHS delineated by the present study and Ito et al. (2017) can be connected at 0–20 km in the X axis, corresponding to a longitude of 141°E (Figs. 4, 5b). We suggest that the upper boundary of the PHS is shallower by approximately 2–6 km than that reported by Uchida et al. (2010) in the area 140.5°E–141.5°E and 35°N–35.5°N. In the landward area, the upper boundaries estimated by the present study coincide with those of Uchida et al. (2010) at a depth of 30 km. The upper boundary of the PHS delineated by the present study is consistent with that compiled by Kono et al. (2017) at 15 km depth (Fig. 5b). The boundary is shallower than that by Kono et al. (2017) at the greater depths, perhaps because the Kono et al.'s iso-depth at 20 km depth was delineated by a land-based study (Hirose et al. 2008).

Low-velocity and low- V_p/V_s anomalies in the NA plate

A striking feature of the tomographic image is the localized and pronounced low-velocity and low- V_p/V_s anomalies at depths shallower than 20 km in the NA plate. The seismicity is very low in the areas with low-velocity anomalies and high along the western edge of the anomalies (Fig. 3).

Low-velocity anomalies in the overriding plate beneath a subduction zone can often be attributed to the presence of fluid. A tomographic study by Yamamoto et al. (2014) found that the velocity decrease of the upper crust and V_p/V_s ratio of higher than 1.8. They suggested that water expelled from the subducting PAC moves upward into the landward upper crust beneath a region off Miyagi. While the velocities and location of the low-velocity anomaly off Miyagi were similar to those obtained in the present study, the V_p/V_s ratio off the Boso Peninsula is low in contrast to the high V_p/V_s ratio off Miyagi.

A compositional anomaly in the crust of the overriding NA plate may be necessary for the V_p/V_s ratio to be low. Rocks with a low- V_p/V_s ratio are probably concentrated in the crust of the overriding plate. Quartz is one of the primary minerals in a continental crust with very low- V_p/V_s values. Christensen (1996) reported that quartzite has V_p , V_s , and V_p/V_s values of approximately 6.0, 4.0, and 1.5 km/s, respectively, as determined by velocity measurements performed in the laboratory. While the velocities estimated in the present study (V_p of 4.4–5.5 km/s and V_s of 2.8–3.5 km/s) are lower than those of quartzite, the difference may be explained by the existence of a fluid. Thus, the shallow low-velocity anomaly may indicate both the presence of quartzite in a locally concentration and water expelled from the subducted PHS and PAC.

A low- V_p/V_s ratio in the overriding crust has also been reported in the case of the Cascadia subduction zone. Ramachandran and Hyndman (2012) detected a region with a low Poisson's ratio (0.22; which is equivalent to a V_p/V_s ratio of 1.65) at depths of 30–35 km in the forearc crust using seismic tomography. The temperature is 400 °C at this depth (Hyndman and Wang 1995). They suggested that the low Poisson's ratio meant the presence of quartzite deposited from the fluids released from the subducted Cascadia slab. It is unknown that the phenomena associated with subduction of the young and warm Cascadia slab could occur off the Boso Peninsula, where the subducted PHS (the former Izu-Bonin forearc) is older than 35 Ma (Ishizuka et al. 2011). It will be important to examine the thermal structure off the Boso Peninsula in order to determine whether the quartz deposition process could occur.

Conclusions

We determined the three-dimensional seismic structure of the crust and upper mantle off the Boso Peninsula using data by ocean-bottom seismographs and land stations from 2011 to 2013.

Based on the obtained tomographic image and the hypocenter distribution and focal mechanisms determined by Ito et al. (2017), we propose new geometry for the upper boundary of the PHS, locating it in the area 140.5°E–141.5°E and 35°N–35.5°N. The upper boundary of the PHS is 2–6 km shallower than that reported by Uchida et al. (2010).

Significant low-velocity and low- V_p/V_s anomalies were observed at depths shallower than 20 km in the overriding NA. These anomalies may be caused by the presence of quartzite and the water expelled from the subducted PAC and PHS.

Additional file

Additional file 1: Table A1. Observation period and the number of seismic stations used in this study. **Additional note 1.** Calculation of the station correction. **Figure A1.** Example of PS converted phases observed at station 1 (Figure A2). **Figure A2.** Seismic stations and crustal model used for station correction. **Figure A3.** Distribution of station corrections for (a) P and (b) S waves. **Additional note 2.** Parameters during tomographic inversion. **Table A2.** Reduction in the RMS of travel time residuals by tomographic inversion. **Table A3.** Parameters used for tomographic inversions and resultant condition numbers. **Figure A4.** Relationship between travel time residuals and structural amplitude. **Additional note 3.** Checkerboard resolution test. **Figure A5.** Results of the checkerboard resolution test in horizontal section. **Figure A6.** Results of checkerboard resolution test along the X axis shown in Figure 2c. **Figure A7.** Results of checkerboard resolution test along the Y axis shown in Figure 2c.

Abbreviations

OBS: ocean-bottom seismometer; PAC: Pacific plate; NA: North American plate; PHS: Philippine Sea plate; ERI: Earthquake Research Institute; JAMSTEC: Japan Agency of Marine-Earth Science and Technology; NIED: National Research Institute for Earth Science and Disaster Prevention; JMA: Japan Meteorological Agency; DWS: derivative weight sum.

Authors' contributions

AI performed data processing and analysis and wrote the manuscript. YY, RH, DS, and HS suggested improvements in the manuscript. MN and KO helped with the data processing and analysis. KN and MS helped with the OBS data collection by ERI. All authors read and approved the final manuscript.

Author details

¹ Department of Deep Earth Structure and Dynamics Research, Japan Agency of Marine-Earth Science and Technology, 2-15 Natsushima-cho, Yokosuka, Kanagawa 237-0061, Japan. ² Research and Development Center for Earthquake and Tsunami, Japan Agency of Marine-Earth Science and Technology, 3173-25, Showa-machi, Kanazawa-ku, Yokohama, Kanagawa 236-0001, Japan. ³ Research Center for Prediction of Earthquakes and Volcanic Eruptions, Graduate School of Science, Tohoku University, 6-6, Aza-Aoba, Aramaki, Aoba-ku, Sendai, Miyagi 980-8578, Japan. ⁴ Department of Planetology, Graduate School of Science, Kobe University, 1-1 Rokkodai-cho, Nada-ku, Kobe, Hyogo 657-8501, Japan. ⁵ Tokyo University of Marine Science and Technology, 4-5-7, Konan, Minato-ku, Tokyo 108-8477, Japan. ⁶ Earthquake Research Institute, University of Tokyo, 1-1-1, Yayoi, Bunkyo-ku, Tokyo 113-0032, Japan.

Acknowledgements

We used data from the Hi-net and F-net systems operated by NIED and through onshore observations by the JMA.

Competing interests

The authors declare that they have no competing interests.

Publisher's Note

Springer Nature remains neutral with regard to jurisdictional claims in published maps and institutional affiliations.

Received: 12 June 2017 Accepted: 16 August 2017

Published online: 24 August 2017

References

Christensen NI (1996) Poisson's ratio and crustal seismology. *J Geophys Res* 101:3139–3156

DeMets C, Gordon RG, Argus DF (2010) Geologically current plate motions. *Geophys J Int* 118:1–80. doi:10.1111/j.1365-246X.2009.04491.x

Hino R, Ito S, Shiobara H, Shimamura H, Sato T, Kanazawa T, Kasahara J, Hasegawa A (2000) Aftershock distribution of the 1994 Sanriku-oki earthquake (Mw 7.7) revealed by ocean bottom seismographic observation. *J Geophys Res* 105:21697–21710. doi:10.1029/2000JB900174

Hirose F, Nakajima J, Hasegawa A (2008) Three-dimensional velocity Structure and configuration of the Philippine Sea Slab beneath Kanto district, central Japan, estimated by double-difference tomography. *J Seismol Soc Jpn* 60:123–138 (in Japanese)

Hirose H, Matsuzawa T, Kimura T, Kimura H (2014) The Boso slow slip events in 2007 and 2011 as a driving process for the accompanying earthquake swarm. *Geophys Res Lett* 41:2778–2785. doi:10.1002/2014GL059791

Hyndman RD, Wang K (1995) The rupture zone of Cascadia great earthquakes from current deformation and the thermal regime. *J Geophys Res* 100:22133–22154. doi:10.1029/95JB01970

Ishida M (1992) Geometry and relative motion of the Philippine Sea plate and Pacific plate beneath the Kanto-Tokai district, Japan. *J Geophys Res* 97:489–513

Ishizuka O, Tani K, Reagan KM, Kanayama K, Umino S, Harigane Y, Sakamoto I, Miyajima Y, Yuasa M, Dunkley JD (2011) The timescales of subduction initiation and subsequent evolution of an oceanic island arc. *Earth Planet Sci Lett* 306:229–240. doi:10.1016/j.epsl.2011.04.006

Ito A, Sugioka H, Obana K, Hino R, Suetsugu D, Nakahigashi K, Shinohara M, Nakano M, Yamamoto Y (2017) Upper boundaries of the Pacific and Philippine Sea plates near the triple junction off the Boso Peninsula deduced from ocean-bottom seismic observations. *Earth Planets Space* 69:30. doi:10.1186/s40623-017-0608-4

Kamiya S, Kobayashi Y (2000) Seismological evidence for the existence of serpentinized wedge mantle. *Geophys Res Lett* 27:819–822

Kono A, Sato T, Shinohara M, Mochizuki K, Yamada T, Uehira K, Shinbo T, Machida Y, Hino R, Azuma R (2017) Geometry and spatial variations of seismic reflection intensity of the upper surface of the Philippine Sea plate off the Boso Peninsula, Japan. *Tectonophysics* 709:44–54. doi:10.1016/j.tecto.2017.05.001

Lomax A, Virieux J, Volant P, Berge C (2000) Probabilistic earthquake location in 3D and layered models: introduction of a Metropolis–Gibbs method and comparison with linear locations. In: Thurber CH, Rabinowitz N (eds) *Advances in seismic event location*. Kluwer, Amsterdam, pp 101–134

Matsu'ura M, Noda A, Fukahata Y (2007) Geodetic data inversion based on Bayesian formulation with direct and indirect prior information. *Geophys J Int* 171:1342–1351

Matsubara M, Hayashi H, Obara K, Kasahara K (2005) Low-velocity oceanic crust at the top of the Philippine Sea and Pacific plates beneath the Kanto region, central Japan, imaged by seismic tomography. *J Geophys Res* 110:B12304. doi:10.1029/2005JB003673

Nakahigashi K, Shinohara M, Mochizuki K, Yamada T, Hino R, Sato T, Uehira K, Ito Y, Murai Y, Kanazawa T (2012) P-wave velocity structure in the southernmost source region of the 2011 Tohoku earthquakes, off the Boso Peninsula deduced by an ocean bottom seismographic survey. *Earth Planets Space* 64:1149–1156. doi:10.5047/eps2012.06.006

Nakajima J, Hirose F, Hasegawa A (2009) Seismotectonics beneath the Tokyo metropolitan area, Japan: effect of slab–slab contact and overlap on seismicity. *J Geophys Res* 114:B08309. doi:10.1029/2008JB006101

Okada Y, Kasahara K, Hori S, Obara K, Sekiguchi S, Fujiwara H, Yamamoto A (2004) Recent progress of seismic observation networks in Japan—Hi-net, F-net, K-NET and KiK-net. *Earth Planets Space* 56:xv–xxviii. doi:10.1186/BF03353076

Ramachandran K, Hyndman RD (2012) The fate of fluids released from subducting slab in northern Cascadia. *Solid Earth* 3:121–129. doi:10.5194/se-3-121-2012

Sato T, Higuchi H, Miyauchi T, Endo K, Tsumura N, Ito T, Noda A, Matsu'ura M (2016) The source model and recurrence interval of Genroku-type Kanto earthquakes estimated from paleo-shoreline data. *Earth Planets Space* 68:17. doi:10.1186/s40623-016-0395-3

Shinohara M, Machida Y, Yamada T, Nakahigashi K, Shinbo T, Mochizuki K, Murai Y, Hino R, Ito Y, Sato T, Shiobara H, Uehira K, Yakiwara H, Obana K, Takahashi N, Kodaira S, Hirata K, Tsushima H, Iwasaki T (2012) Precise aftershock distribution of the 2011 off the Pacific coast of Tohoku Earthquake revealed by an ocean-bottom seismometer network. *Earth Planets Space* 64:1137–1148. doi:10.5047/eps.2012.09.003

- Spakman W, Nolet G (1988) Imaging algorithms, accuracy and resolution in delay time tomography. In: Vlarr N et al (eds) *Mathematical geophysics*. D. Reidel, Norwell, pp 155–187
- Thurber CH, Eberhart-Phillips D (1999) Local earthquake tomography with flexible gridding. *Comput Geosci* 25:809–818
- Uchida N, Nakajima J, Hasegawa A, Matsuzawa T (2009) What controls inter-plate coupling?: evidence for abrupt change in coupling across a border between two overlying plates in the NE Japan subduction zone. *Earth Planet Sci Lett* 283:111–121
- Uchida N, Matsuzawa T, Nakajima J, Hasegawa A (2010) Subduction of a wedge-shaped Philippine Sea plate beneath Kanto, central Japan, estimated from converted waves and small repeating earthquakes. *J Geophys Res* 115:B07309. doi:[10.1029/2009JB006797](https://doi.org/10.1029/2009JB006797)
- Ueno H, Hatakeyama S, Aketagawa T, Funasaki J, Hamada N (2002) Improvement of hypocenter determination procedures in the Japan Meteorological Agency. *Q J Seismol* 65:123–134 (**in Japanese with English abstract**)
- Waldhauser F, Ellsworth WL (2000) A double-difference earthquake location algorithm: method and application to the northern Hayward fault. *Bull Seismol Soc Am* 90:1353–1368
- Yamamoto Y, Obana K, Kodaira S, Hino R, Shinohara M (2014) Structural heterogeneities around the megathrust zone of the 2011 Tohoku earthquake from tomographic inversion of onshore and offshore seismic observations. *J Geophys Res* 119:1165–1180. doi:[10.1002/2013JB010582](https://doi.org/10.1002/2013JB010582)
- Zhang H, Thurber CH (2003) Double-difference tomography: the method and its application to the Hayward fault, California. *Bull Seismol Soc Am* 93:1875–1889

Submit your manuscript to a SpringerOpen[®] journal and benefit from:

- Convenient online submission
- Rigorous peer review
- Open access: articles freely available online
- High visibility within the field
- Retaining the copyright to your article

Submit your next manuscript at ► springeropen.com
